Supporting information for:

Immobilization Strategies for Enhancing Sensitivity of Electrochemical Aptamer-Based Sensors

Yingzhu Liu†, Juan Canoura†, Obtin Alkhamis and Yi Xiao*

Department of Chemistry and Biochemistry, Florida International University, 11200 SW 8th Street, Miami, FL, 33199.

†These authors contributed equally to this work.
*Corresponding author: yxiao2@fiu.edu

Table of Contents

Table S1. ITC parameters and conditions used in this work and the calculated K_Ds. pH of the buffer is 7.4 unless stated otherwise.

Cell content	Syringe content	Buffer	K_D (μM)
20 μM SC-34	400 μM (-)-MDPV	Low-salt Tris	0.33 ± 0.04
20 μM SC-34	400 μM (-)-MDPV	Low-salt PBS	0.38 ± 0.03
20 μM SC-34	350 μM (-)-MDPV	Low-salt PBS (pH 6.0)	0.23 ± 0.02
20 μM SC-34	350 μM (-)-MDPV	Low-salt PBS (pH 7.0)	0.38 ± 0.02
20 μM SC-34	350 μM (-)-MDPV	Low-salt PBS (pH 7.4)	0.56 ± 0.03
20 μM SC-34	350 μM (-)-MDPV	Low-salt PBS (pH 8.0)	0.69 ± 0.03
20 μM SC-34	300 μM (-)-MDPV	High-salt Tris	1.80 ± 0.05
20 μM SC-34	200 μM (-)-MDPV (2×, back-to-back)	High-salt PBS	1.50 ± 0.04
20 μM COC-32	800 μM cocaine	Low-salt Tris	5.8 ± 0.3
20 μM COC-32	800 μM cocaine	Low-salt PBS	5.9 ± 0.3
80 μM COC-32	4000 μM cocaine	High-salt PBS	70.4 ± 0.8
20 μM ADE-25	1200 μM adenosine (2×, back-to-back)	Low-salt Tris	K_{D1} = 7.4 ± 0.1 K_{D2} = 103 ± 0.5 $K_{1/2}$ = 27.6 ± 0.2
20 μM ADE-25	2500 μM Adenosine	High-salt PBS	K_{D1} = 36.7 ± 2.4 K_{D2} = 14.5 ± 0.6 $K_{1/2}$ = 23.1 ± 0.8

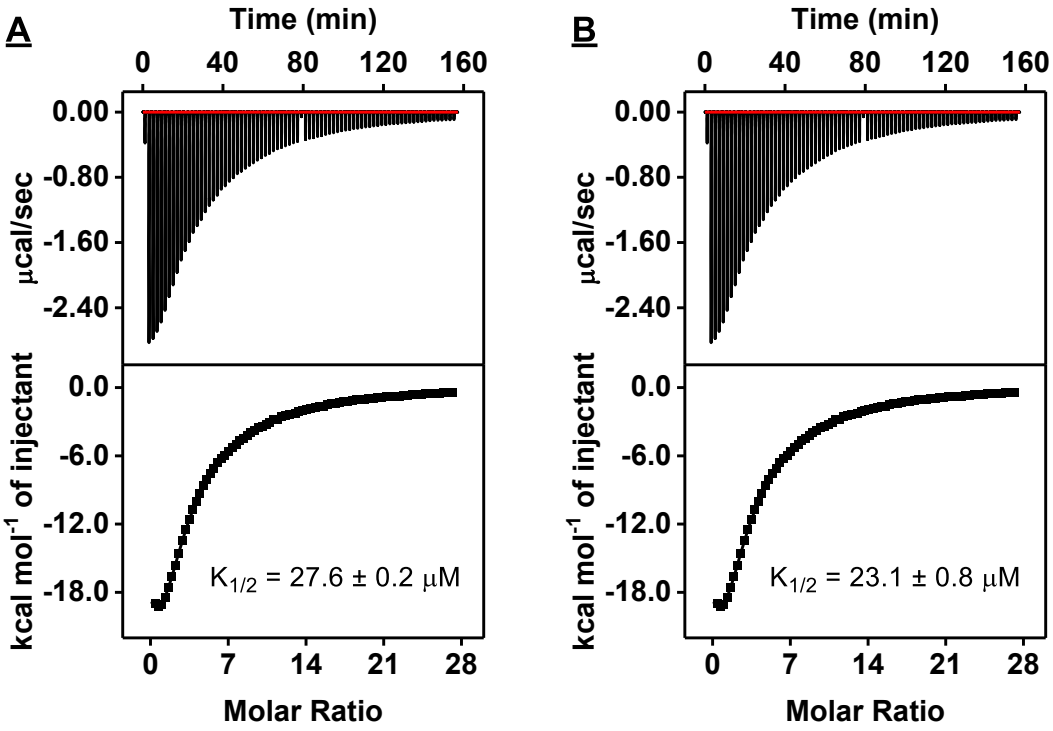

Figure S1. Characterization of the affinity of ADE-25 for adenosine using isothermal titration calorimetry (ITC). Top panels present raw data showing the heat generated from each titration of adenosine to ADE-25 in (**A**) low-salt Tris buffer (10 mM Tris-HCl, 20 mM NaCl, 0.5 mM $MgCl_2$, pH 7.4) or (**B**) high-salt PBS (1.6 mM NaH_2PO_4, 8.4 mM Na_2HPO_4, 1 M NaCl, 1 mM $MgCl_2$, pH 7.2), while bottom panels show the integrated heat of each titration after correcting for dilution heat of the titrant. ITC data were fitted with a two-site sequential binding model. $K_{1/2} = (K_{D1} \times K_{D2})^{1/2}$

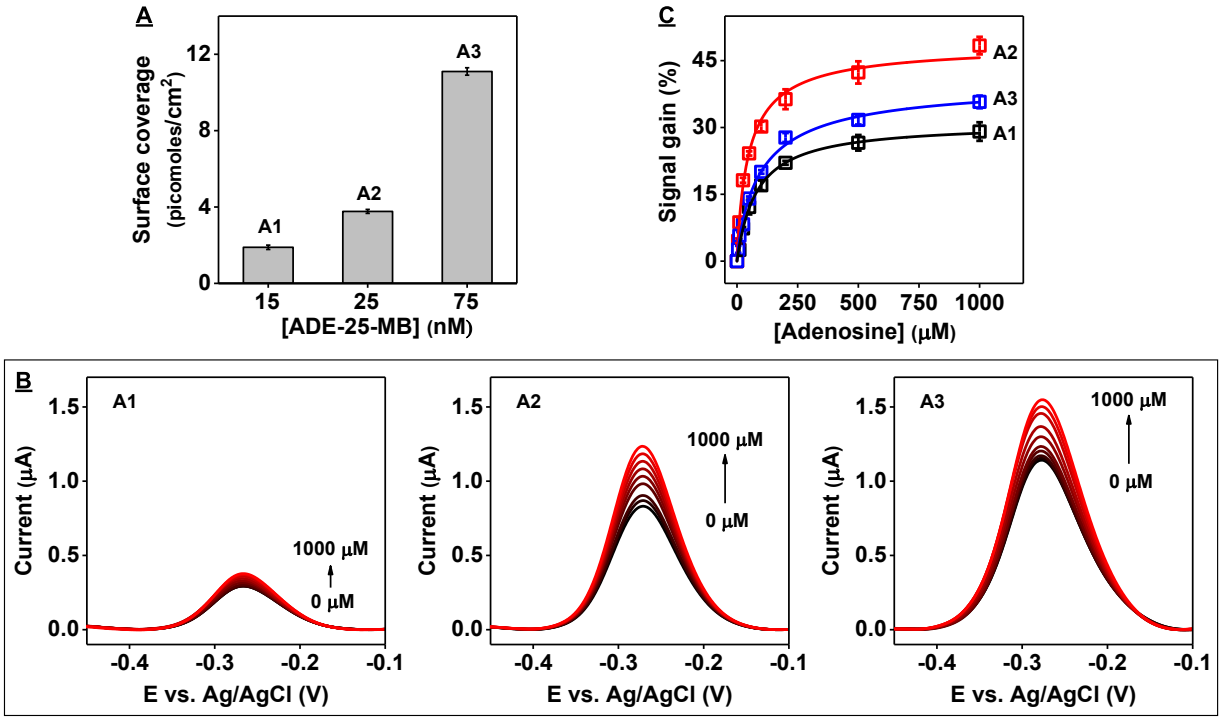

Figure S2. Adenosine detection with electrodes modified with ADE-25-MB using the conventional immobilization approach. (**A**) Aptamer surface coverage of electrodes fabricated using 15 nM (A1), 25 nM (A2), or 75 nM (A3) ADE-25-MB in the absence of target. (**B**) Square wave voltammograms (SWV) and (**C**) calibration curves for adenosine detection produced by the different E-AB sensors with 0 – 1,000 μM adenosine. Error bars represent the standard deviation of measurements from three independently fabricated electrodes.

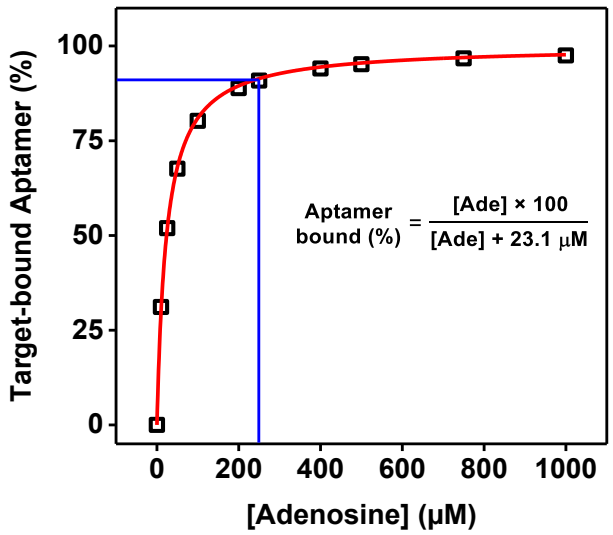

Figure S3. Simulated binding curve for ADE-25 based on its affinity for adenosine in high-salt PBS ($K_{1/2}$ = 23.1 μM). Blue lines indicate that ~91% of the aptamer is bound in the presence of 250 μM adenosine.

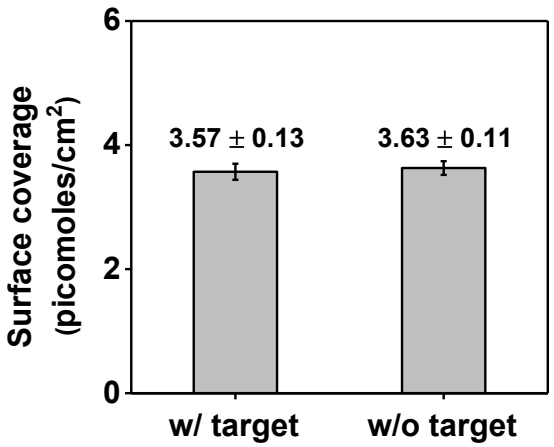

Figure S4. Aptamer surface coverages of electrodes fabricated by immobilizing the aptamer in the presence or absence of 250 μM adenosine. Error bars represent the standard deviation of measurements from three independently fabricated electrodes.

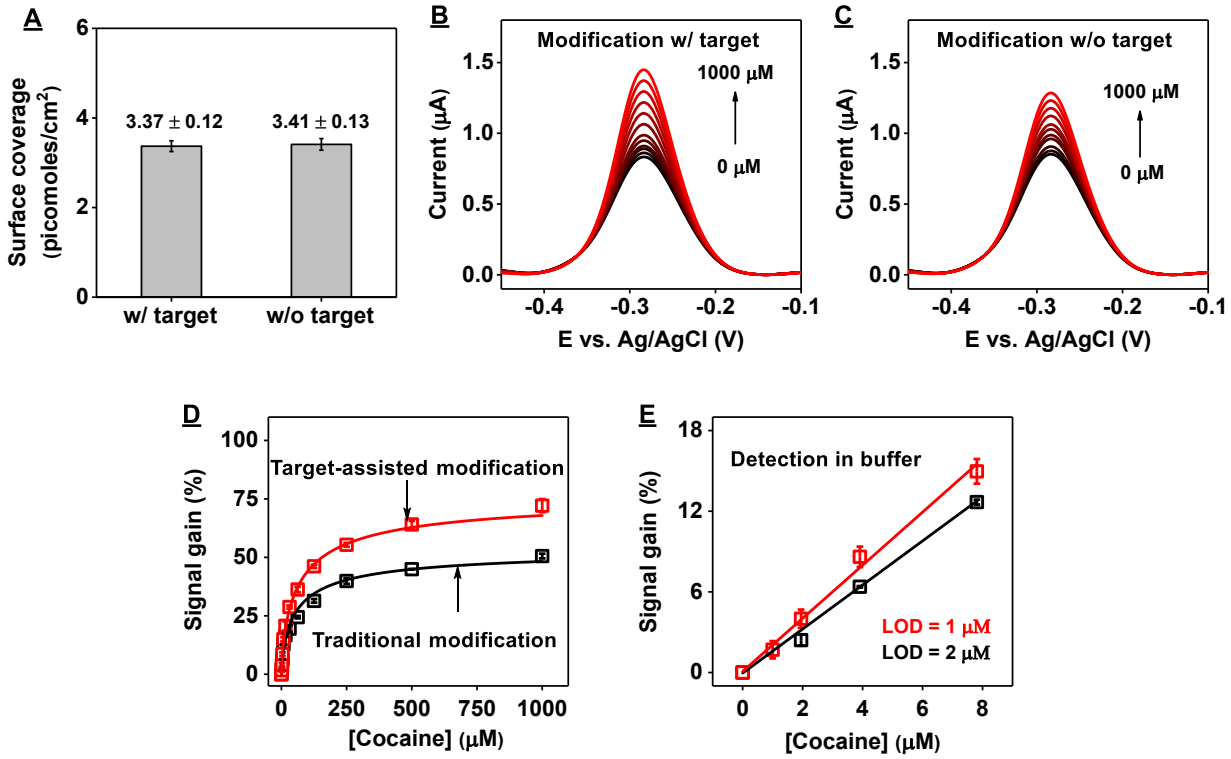

Figure S5. Performance of electrodes fabricated with COC-32-MB via target-assisted immobilization or conventional means in high-salt PBS. (**A**) Surface coverage of electrodes fabricated by immobilizing the aptamer in the presence (w/ target) or absence (w/o target) of 250 μM cocaine. SWV from electrodes fabricated via (**B**) target-assisted immobilization or (**C**) traditional means (aptamer only) and challenged with 0–1000 μM cocaine. (**D**) Calibration curves for detection of cocaine derived from the spectra shown in **B** (red) and **C** (black). (**E**) Sensitivity and LOD of electrodes fabricated using target-assisted immobilization (red) or traditional means (black). Error bars represent the standard deviation of measurements from three independently fabricated electrodes.

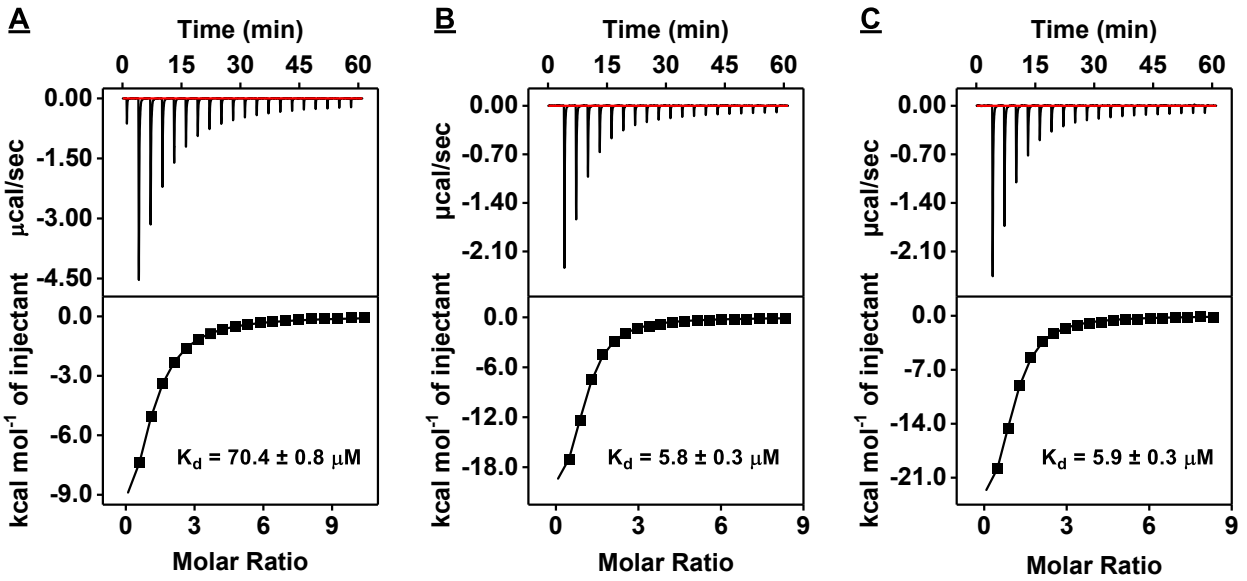

Figure S6. Characterization of the affinity of COC-32 for cocaine using ITC. Top panels present raw data showing the heat generated from each titration of cocaine to COC-32 in (**A**) high-salt PBS, (**B**) low-salt PBS, or (**C**) low-salt Tris buffer, while bottom panels show the integrated heat of each titration after correcting for dilution heat of the titrant. ITC data were fitted with a single-site binding model.

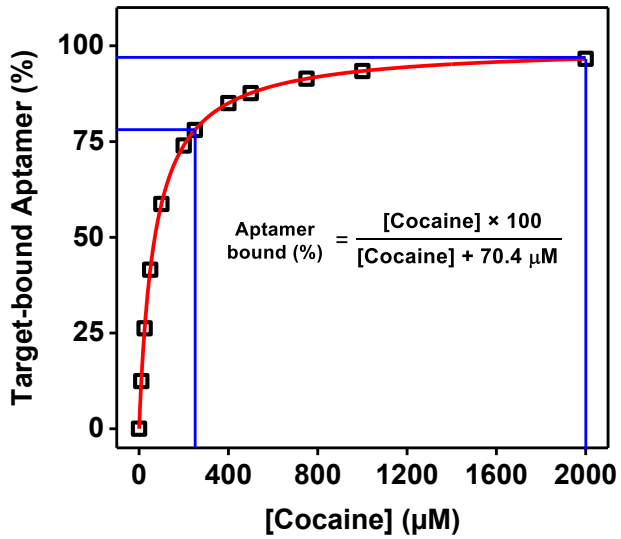

Figure S7. Simulated binding curve for COC-32 based on its affinity for cocaine in high-salt PBS (K_D = 70.4 µM). The blue lines indicate that ~78% and 96% of the aptamer is bound in the presence of 250 µM and 2 mM cocaine, respectively.

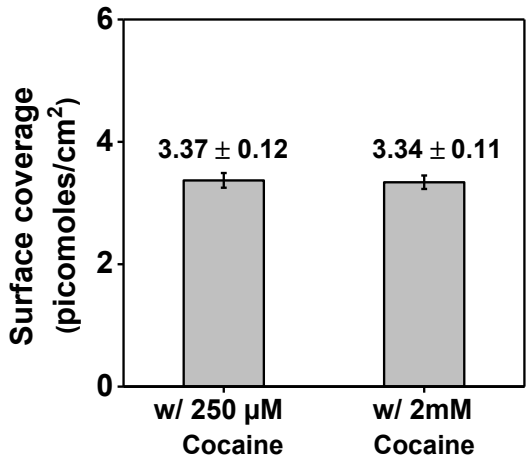

Figure S8. Surface coverage of electrodes modified with COC-32-MB via target-assisted immobilization in high-salt PBS in the presence of 250 µM or 2 mM cocaine. Error bars represent the standard deviation of measurements from three different electrodes.

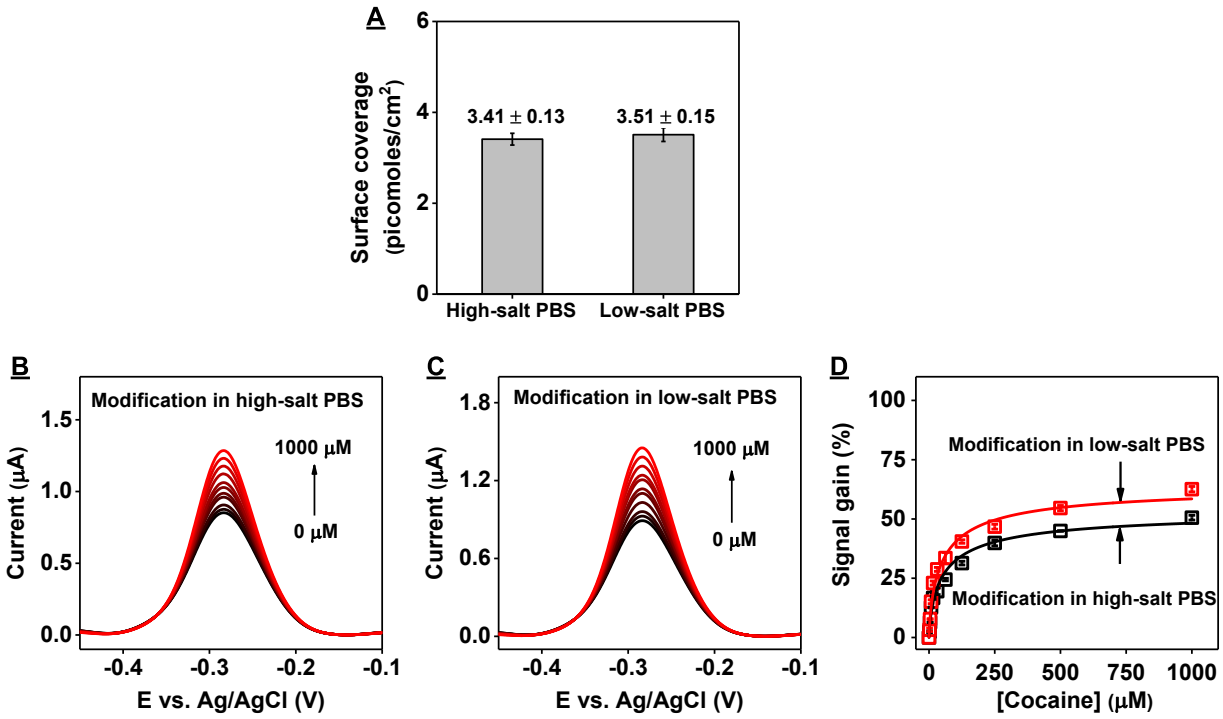

Figure S9. Performance of electrodes fabricated with COC-32-MB via conventional means in different buffers. (**A**) Surface coverage of electrodes fabricated by immobilizing the aptamer in high-salt or low-salt PBS. SWV produced by challenging electrodes fabricated in (**B**) high-salt or (**C**) low-salt PBS with 0–1000 µM cocaine. (**D**) Calibration curves for detection of cocaine derived from the spectra shown in **B** (black) and **C** (red). Error bars represent the standard deviation of measurements from three independently fabricated electrodes.

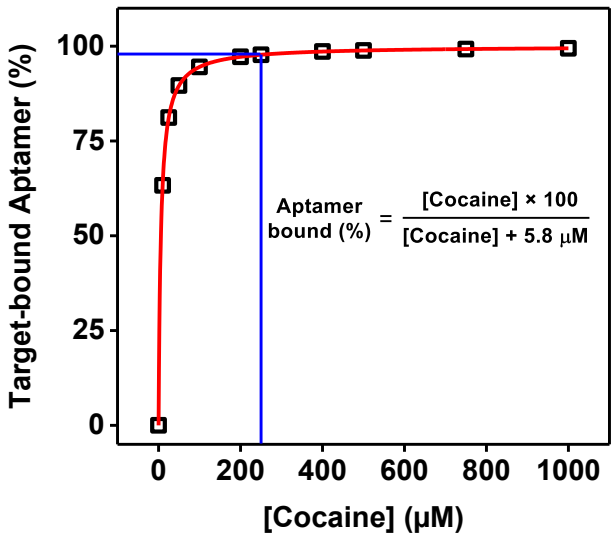

Figure S10. Simulated binding curve for COC-32 based on the affinity for cocaine in low-salt PBS (K_D = 5.8 μM). The blue lines indicate that 96% of the aptamer is bound in the presence of 250 μM cocaine.

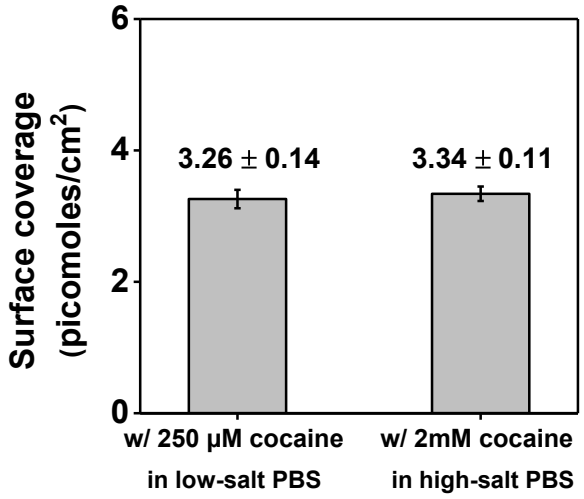

Figure S11. Surface coverage of electrodes modified with COC-32-MB via target-assisted immobilization in low-salt PBS with 250 μM or in high-salt PBS with 2 mM cocaine. Error bars represent the standard deviation of measurements from three different electrodes.

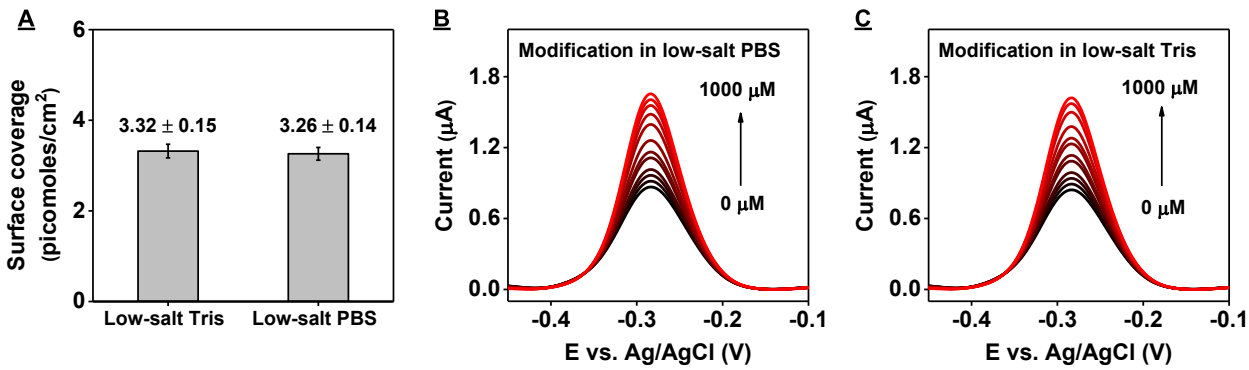

Figure S12. Performance of electrodes fabricated with COC-32-MB via target-assisted immobilization in different buffers. (**A**) Aptamer surface coverages of electrodes fabricated by immobilizing the aptamer in low-salt Tris buffer or low-salt PBS with 250 μM cocaine. SWV produced by challenging the electrodes fabricated in low-salt (**B**) PBS or (**C**) Tris buffer with 0–1000 μM cocaine. Error bars represent the standard deviation of measurements from three independently fabricated electrodes.

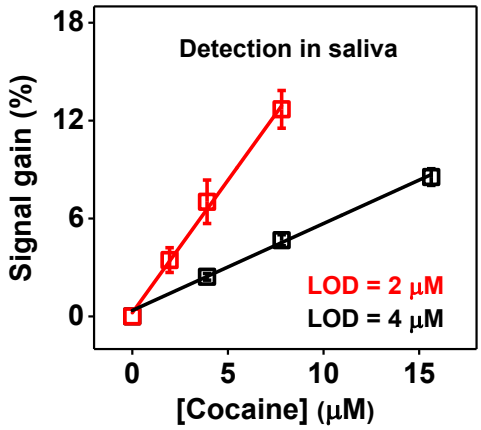

Figure S13. Sensitivity and LOD for cocaine detection in 50% saliva with electrodes fabricated using COC-32-MB via target-assisted immobilization in low-salt Tris buffer with 250 μM cocaine (red) or conventional means in high-salt PBS (black). Error bars represent the standard deviation of measurements from three independently fabricated electrodes.

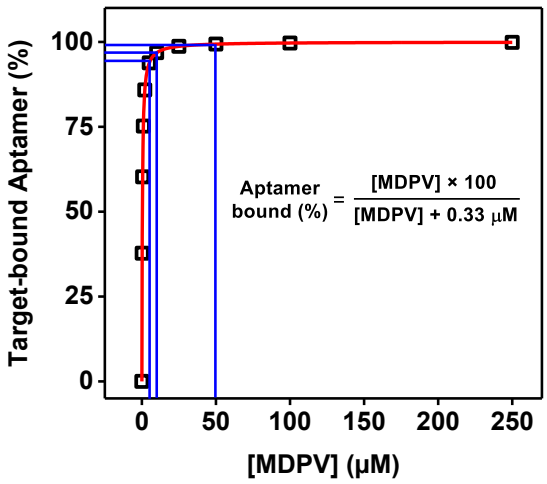

Figure S14. Simulated binding curve for SC-34 based on affinity for MDPV in low-salt Tris buffer (K_D = 0.33 μM). The blue lines indicate that 94%, 97%, and 99% of the aptamer is bound in the presence of 5, 10, and 50 μM MDPV, respectively.

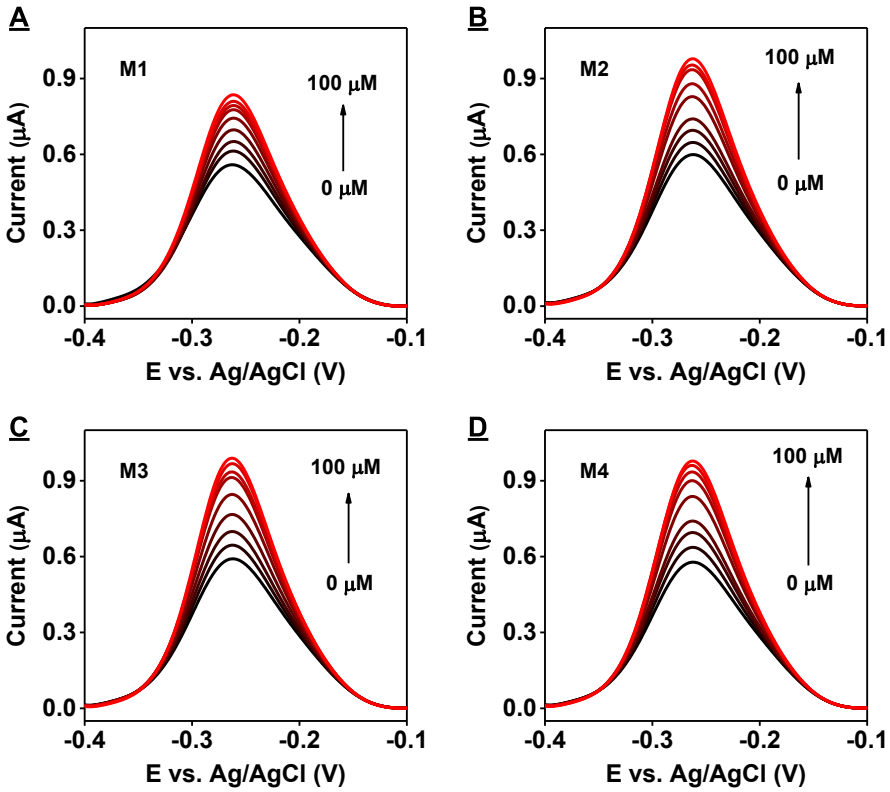

Figure S15. Electrodes fabricated using SC-34-MB via target-assisted aptamer immobilization with various concentrations of MDPV. SWV for electrodes modified with SC-34-MB in the presence of (**A**) 0 μM, (**B**) 5 μM, (**C**) 10 μM, and (**D**) 50 μM MDPV after challenging with 0–100 μM MDPV.

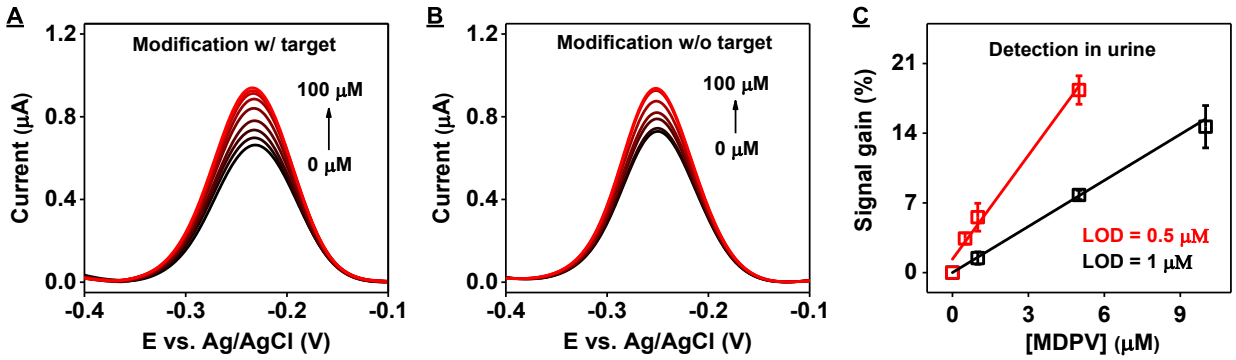

Figure S16. Detection of MDPV in 50% urine using electrodes modified with SC-34-MB via (**A**) target-assisted immobilization in low-salt Tris buffer with 50 μM MDPV or (**B**) conventional means in high-salt PBS. (**C**) Calibration curves derived from spectra shown in **A** (red) and **B** (black). Error bars represent the standard deviation of measurements from three independently fabricated electrodes.

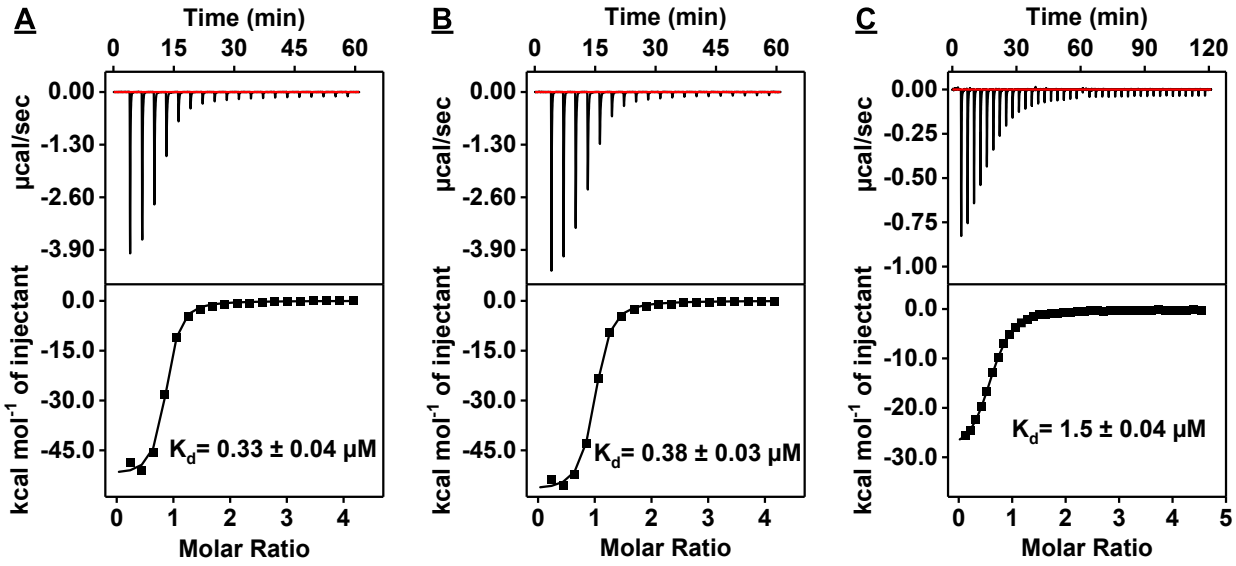

Figure S17. Characterization of the affinity of SC-34 for MDPV using ITC. Top panels present raw data showing the heat generated from each titration of MDPV to SC-34 in (**A**) low-salt Tris buffer, (**B**) low-salt PBS, or (**C**) high-salt PBS, while bottom panels show the integrated heat of each titration after correcting for dilution heat of the titrant. ITC data were fitted with a single-site binding model.

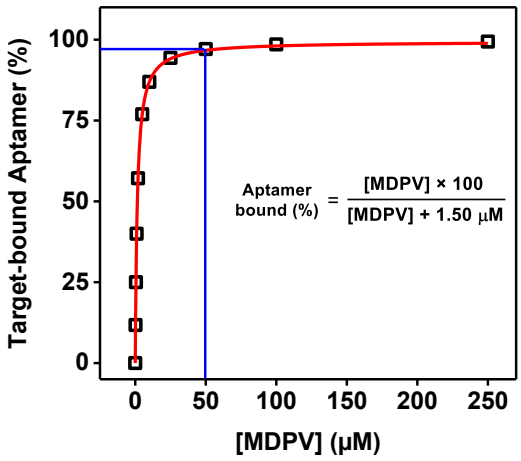

Figure S18. Simulated binding curve for SC-34 based on affinity for MDPV in high-salt PBS (K_D = 1.50 μM). The blue lines indicate that 97% of the aptamer is bound in the presence of 50 μM MDPV.

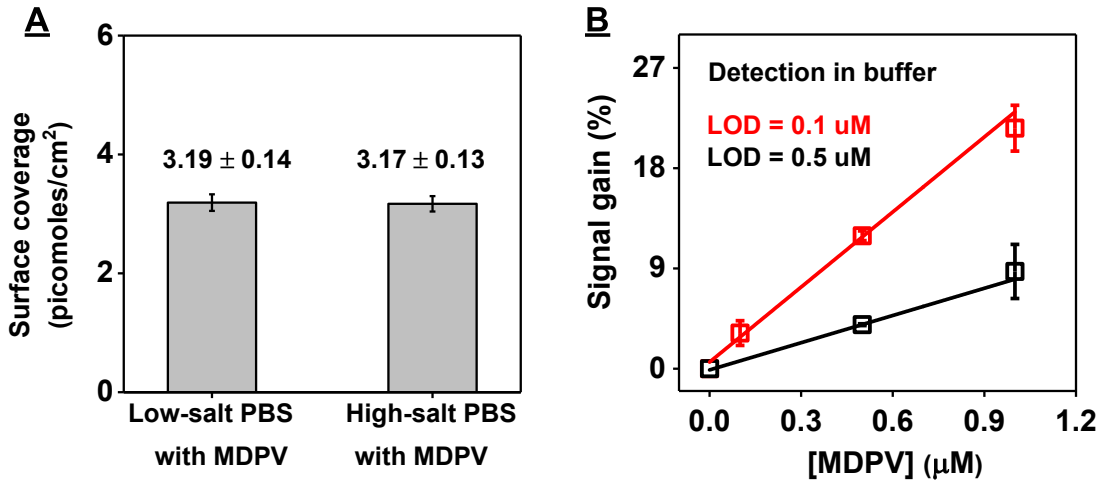

Figure S19. Performance of electrodes fabricated with SC-34-MB via target-assisted immobilization in different buffers. (**A**) Surface coverage of electrodes fabricated by immobilizing the aptamer in low-salt or high-salt PBS with 50 μM MDPV. (**B**) Calibration curve and LOD for MDPV detection using electrodes modified with SC-34-MB via target-assisted immobilization in low-salt (red) or high-salt PBS (black). Error bars represent the standard deviation of measurements from three independently fabricated electrodes.

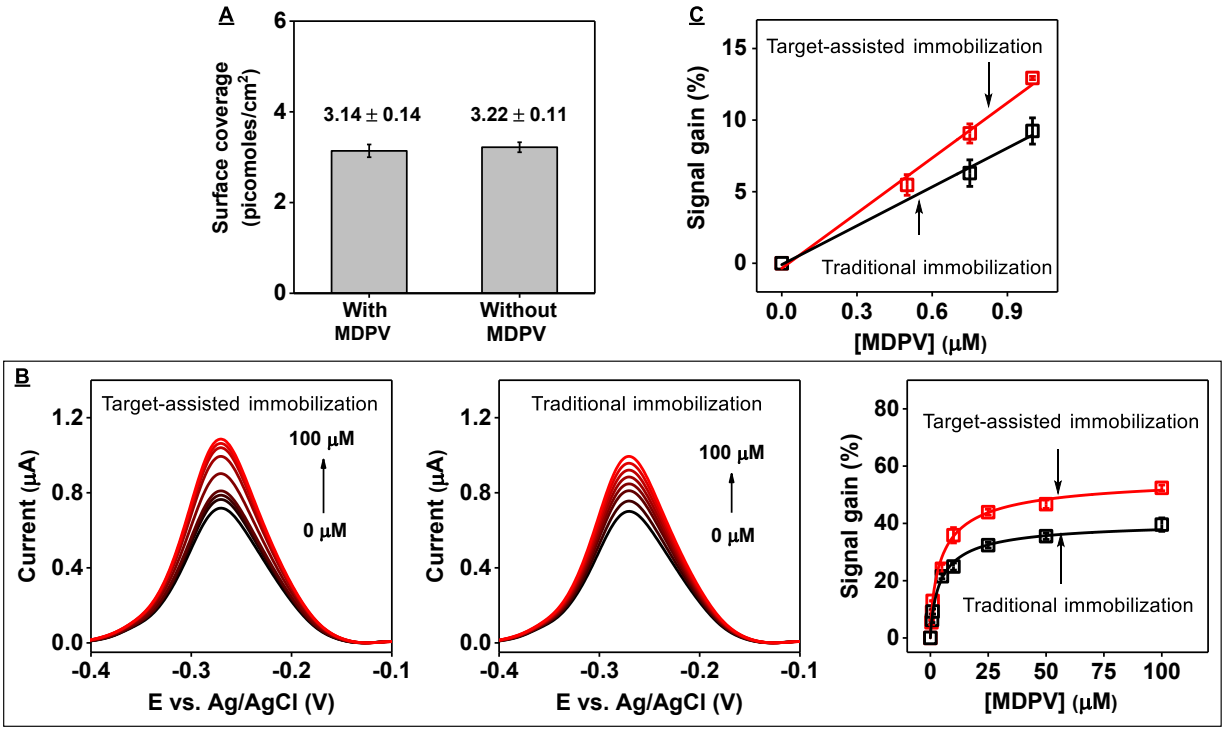

Figure S20. Performance of electrodes fabricated with SC-34-MB in the presence or absence of 50 μM MDPV in high-salt Tris buffer. (**A**) Aptamer surface coverage of fabricated electrodes. (**B**) SWV measurements from electrodes fabricated via target-assisted aptamer immobilization approach (left) or traditional aptamer immobilization (middle) in the presence of 0–1000 μM MDPV. The derived calibration curve is shown at right. (**C**) Linear ranges from the curves shown in B. Error bars represent the standard deviation of measurements from three independently fabricated electrodes.

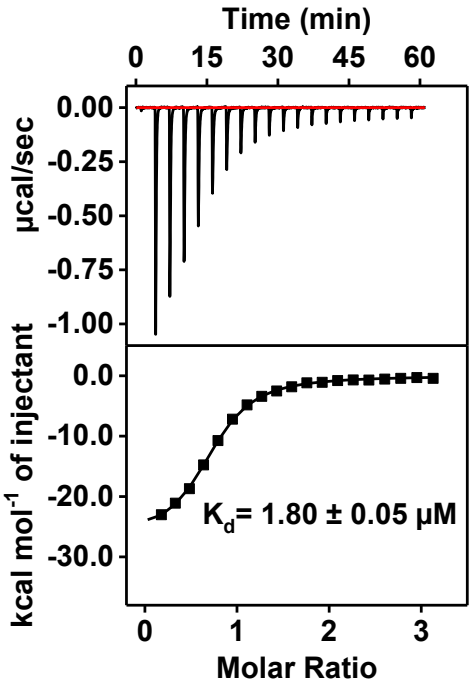

Figure S21. ITC characterization of SC-34 affinity for MDPV in high-salt Tris buffer. Top panels present raw data, showing the heat generated from each titration of MDPV to SC-34, while bottom panels show the integrated heat of each titration after correcting for dilution heat of the titrant. ITC data were fitted with a single-site binding model.

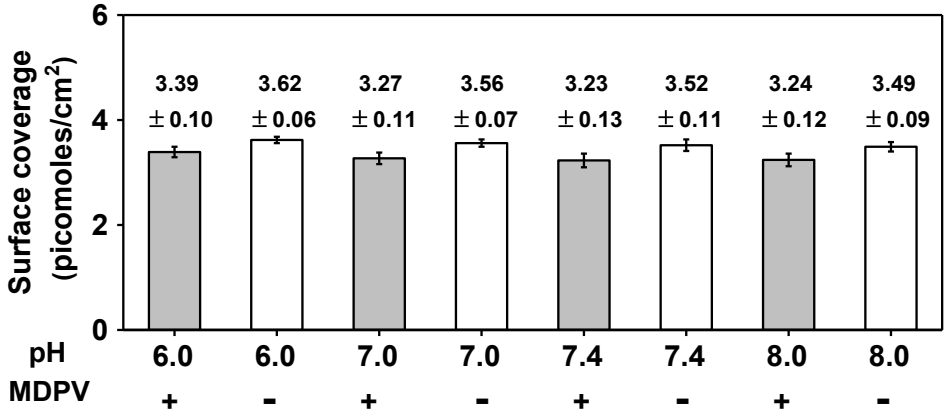

Figure S22. Aptamer surface coverages of electrodes fabricated with SC-34-MB in the absence (white bars) or presence of 50 µM MDPV (gray bars) in low-salt PBS with a pH of 6.0, 7.0, 7.4 or 8.0. Error bars represent the standard deviation of measurements from three independently fabricated electrodes.

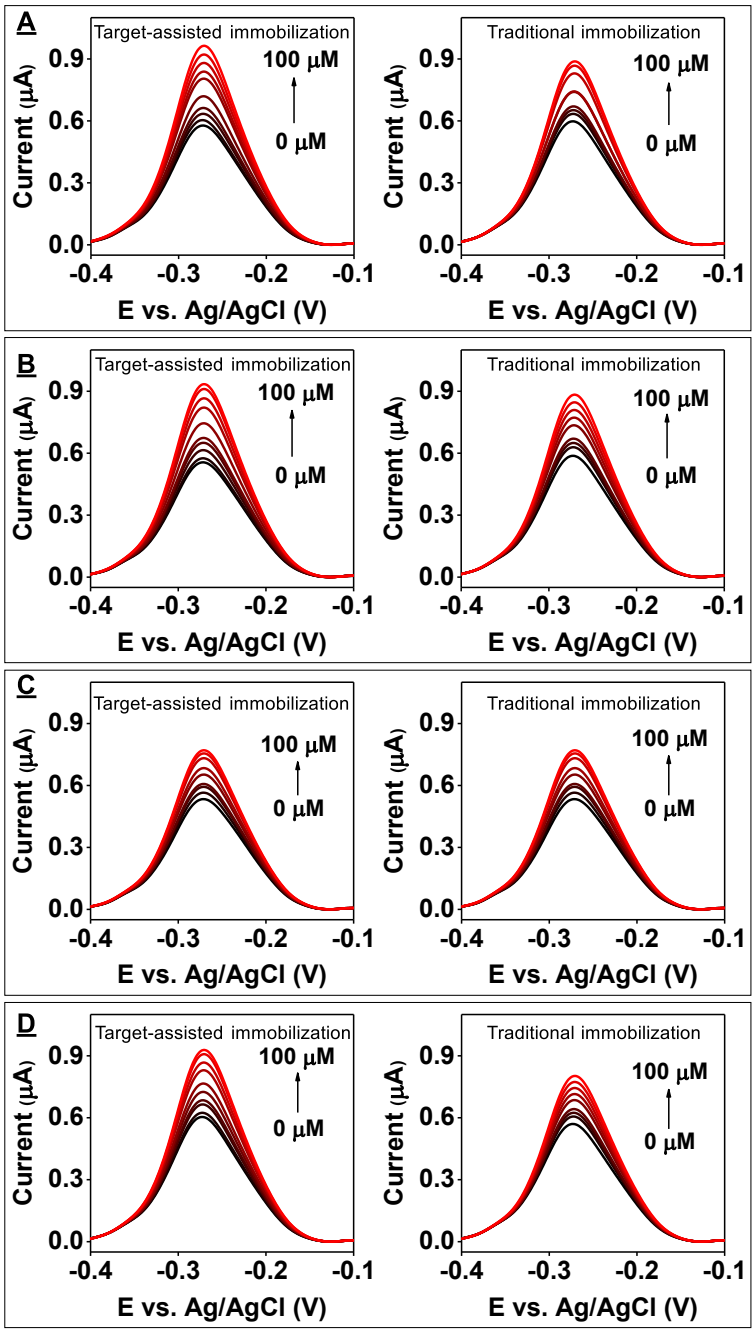

Figure S23. E-AB sensor performance using electrodes modified with SC-34-MB in the presence (target-assisted immobilization) or absence (traditional immobilization) of 50 µM MDPV in low-salt PBS at pH (**A**) 8.0, (**B**) 7.4, (**C**) 7.0 and (**D**) 6.0. SWV spectra for electrodes prepared under these two immobilization conditions and then exposed to 0–100 µM MDPV. Error bars represent the standard deviation of measurements from three independently fabricated electrodes.

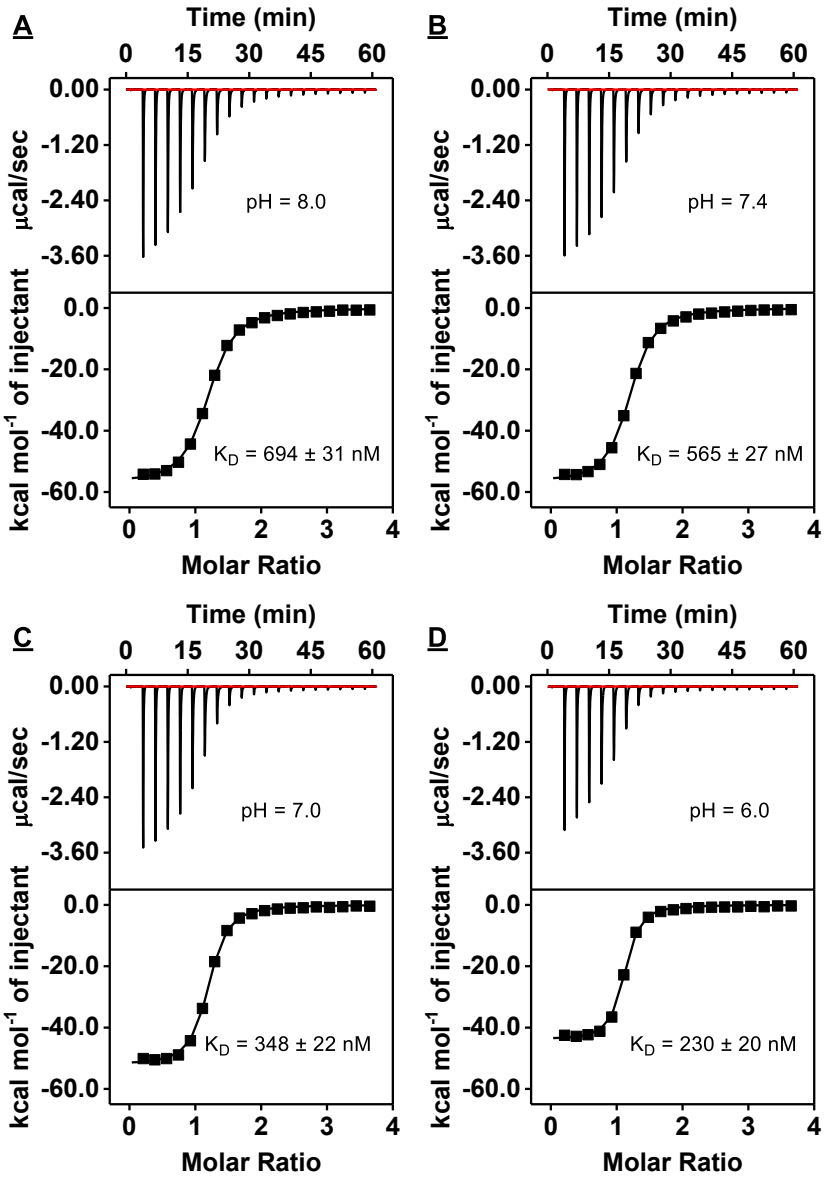

Figure S24. Characterization of the pH-dependence of SC-34 affinity for MDPV using ITC. Top panels present raw data showing the heat generated from each titration of MDPV to SC-34 in low-salt PBS at pH (**A**) 8.0, (**B**) 7.4, (**C**) 7.0, or (**D**) 6.0, while bottom panels show the integrated heat of each titration after correcting for dilution heat of the titrant. ITC data were fitted with a single-site binding model.